Available online at www.sciencedirect.com
SCIENCE DIRECT
ELSEVIER
Solid State Communications 132 (2004) 141–149
solid state communications
www.elsevier.com/locate/ssc

Research Paper

Exact envelope-function theory versus symmetrized Hamiltonian for quantum wires: a comparison

B. Lassen[a], L.C. Lew Yan Voon[b,*], M. Willatzen[a], R. Melnik[a]

[a]*Mads Clausen Institute, The University of Southern Denmark, Grundvigs Alle 150, DK-6400 Sønderborg, Denmark*
[b]*Department of Physics, Worcester Polytechnic Institute, 100 Institute Road, Worcester, MA 01609, USA*

Received 19 July 2004; accepted 20 July 2004 by M. Cardona
Available online 3 August 2004

Abstract

We study the influence of shape, orientation, size and material system on the band structure of quantum wires with special attention given to the differences between results obtained with the Burt–Foreman and the Luttinger–Kohn Hamiltonians. We also show how to derive the Hamiltonians for an arbitrary orientation. We find that the difference is independent of the shape and orientation of the quantum wire, but it does depend on the size and the material system chosen. A brief discussion of the results in terms of group theory is provided.

PACS: 71. 15.−m; 73.61.Ey; 73.61. Tm

Keywords: A. Quantum wires; A. Nanostructures; E. k·p theory; E. Luttinger–Kohn; E. Burt–Foreman; A. III–V Semiconductors; D. Orientation

1. Introduction

One of the most computationally inexpensive classes of models to describe nanoscale semiconductor heterostructures is the multiband models based on some sort of envelope-function theory [1,2]. The main problem within this class of models is to define suitable interface boundary conditions. The method most often used is to symmetrize the bulk multiband Hamiltonian. Burt, however, has derived a theory [1] (exact envelope-function theory) which naturally gives the right interface boundary conditions. The resulting Hamiltonian is called the Burt–Foreman (BF) Hamiltonian.

Before now a comparison between the BF and the symmetrized model has only been carried out for quantum wells [3,4] and spherical dots [5] and, in the latter case, they made some extra approximations in order to get a one-dimensional problem. All of these show differences between the results obtained with the two models. Meney et al. [3] even showed that the BF Hamiltonian gives more physically plausible results and Pokatilov et al. [5] showed that the difference is proportional to one over the radius squared, i.e. the difference will be more pronounced for small structures. In this article we investigate amongst other things whether the difference between the two models also has a size dependence for quantum wires.

For quantum wells and wires a parameter of some importance is the orientation. This is mainly due to the fact that the microscopic symmetry changes with respect to the orientation. van Dalen et al. [6] have derived the operator ordering according to the exact envelope-function theory for an arbitrary orientation for quantum wells. We show how to find the BF Hamiltonian for an arbitrary orientation for quantum wires in a slightly different manner. Another system parameter of some importance is the shape of the quantum wire, again because this changes the overall

* Corresponding author. Fax: +1-508-831-5886.
E-mail address: llew@wpi.edu (L.C. Lew Yan Voon).

0038-1098/$ - see front matter © 2004 Elsevier Ltd. All rights reserved.
doi:10.1016/j.ssc.2004.07.050

symmetry. Dupertuis et al. [7] have made a thorough investigation of this and its consequences. We have chosen to compare three different cross-sectional shapes that have been grown, a circle [8], a square [9,10] and a triangle [11]. Indeed, our study of quantum wires is further motivated by the current interest in their synthesis.

Quantum-wire calculations have until now mainly been carried out using the symmetrized model [12–14]; however, we have previously presented preliminary results using the Burt–Foreman model [15–17]. Here we provide a comparison between the results obtained with the symmetrized and the BF model for a set of different quantum-wire geometries. In Section 2 we present the theoretical framework for this comparison and we highlight the main differences between the two models. Section 3 contains the numerical results and a discussion of the differences observed for the following system characteristics: shape (circle, square, triangle), orientation ([001], [110], [111]), size (circle with a diameter of 6 and 10 nm) and material system (GaAs/AlAs, $In_{0.53}Ga_{0.47}As$/InP). The conclusion is given in Section 4.

2. Theory

2.1. Multiband Hamiltonian

The governing equation for a multiband model is the eigenvalue equation,

$$\mathbf{HF} = E\mathbf{F}, \tag{1}$$

where the Hamiltonian $\mathbf{H}$ is a $N\times N$ matrix of differential operators and $\mathbf{F}$ is a N vector of envelope functions. We study the Hamiltonians resulting from two different approaches to reducing the Schrödinger equation to a multiband equation. The Hamiltonians in question are called the Luttinger–Kohn (LK) and the Burt–Foreman (BF) Hamiltonian, respectively.

The LK Hamiltonian is found by first using $\mathbf{k}\cdot\mathbf{p}$ theory to get an effective-mass equation for a bulk system. This is then extended to a heterostructure by symmetrizing the Hamiltonian with respect to the $\vec{k}$ operator. The reason why this is done is to get a hermitian Hamiltonian but it has no physical justification. The BF Hamiltonian is, on the other hand, derived assuming a heterostructure from the beginning using the exact envelope function theory derived by Burt [1].

The four-band BF Hamiltonian written with respect to the total angular momentum $|JM\rangle$ basis for a zinc-blende crystal structure is given by

$$H_4^{BF,LK} = \frac{\hbar^2}{2m_0}\begin{pmatrix} |\frac{3}{2}\frac{3}{2}\rangle & |\frac{3}{2}\frac{1}{2}\rangle & |\frac{3}{2}-\frac{1}{2}\rangle & |\frac{3}{2}-\frac{3}{2}\rangle \\ P' & S_- & -R & 0 \\ S_-^\dagger & P'' & -C & R \\ -R^\dagger & -C^\dagger & P''* & S_+^\dagger \\ 0 & R^\dagger & S_+ & P'* \end{pmatrix} + E_v$$

where E_v, is the valence-band offset, and

$$P' = \frac{1}{2}\{\hat{k}_x(A+B)\hat{k}_x + \hat{k}_y(A+B)\hat{k}_y + \hat{k}_z 2B\hat{k}_z\}, + \frac{i}{2} \times\{\hat{k}_x(C_1+C_2)\hat{k}_y - \hat{k}_y(C_1+C_2)\hat{k}_x\},$$

$$P'' = \frac{1}{6}\{\hat{k}_x(A+5B)\hat{k}_x + \hat{k}_y(A+5B)\hat{k}_y + \hat{k}_z(4A+2B)\hat{k}_z\} + \frac{i}{6}\{\hat{k}_x(C_1+C_2)\hat{k}_y - \hat{k}_y(C_1+C_2)\hat{k}_x\},$$

$$S_\pm = -\frac{1}{2\sqrt{3}}\{(\hat{k}_x \pm i\hat{k}y) + (C_1-C_2)\hat{k}_z + \hat{k}_z(C_1-C_2) \times(\hat{k}_x \pm i\hat{k}_y)\} - \frac{1}{2\sqrt{3}}\{(\hat{k}_x \pm i\hat{k}_y)(C_1+C_2)\hat{k}_z - \hat{k}_z \times(C_1+C_2)(\hat{k}_x \pm i\hat{k}_y)\},$$

$$R = \frac{1}{2\sqrt{3}}\{\hat{k}_x(A-B)\hat{k}_x + \hat{k}_y(A-B)\hat{k}_y\} - \frac{i}{2\sqrt{3}} \times\{\hat{k}_x(C_1-C_2)\hat{k}_y + \hat{k}_y(C_1-C_2)\hat{k}_x\},$$

$$C = \frac{1}{3}\{(\hat{k}_x - i\hat{k}_y)(C_1+C_2)\hat{k}_z - \hat{k}_z(C_1+C_2)(\hat{k}_x - i\hat{k}_y)\}.$$

The LK Hamiltonian is readily obtained from the BF Hamiltonian by setting the terms containing C_1+C_2 to be zero. To see this notice that, in the bulk case, all the terms proportional to C_1+C_2 cancel out and when the resulting Hamiltonian is symmetrized all the terms except the ones proportional to C_1+C_2 reappear. For numerical values of the coefficients we used in the calculations see Table 1.

From the above, we can draw two conclusions already.

Table 1
Material parameters

	E_v [eV]	γ_1	γ_2	γ_3	C_1+C_2
GaAs [18]	−0.4988	6.85	2.10	2.90	−10.10
AlAs [18]	0	3.45	0.68	1.29	−1.56
InP [19]	0	4.95	1.65	2.35	−8.80
$In_{0.53}Ga_{0.47}As$ [19]	−0.3903	14.03	5.39	6.19	−28.64

First, we observe that for a quantum wire there are differences between BF and LK even at the Brillouin zone center. Second, the difference between the two models is characterized by the step function C_1+C_2 alone such that the models are identical if C_1+C_2 is a constant over the whole structure.

2.2. Boundary conditions

We are only interested in the bound states in the structure so we impose Dirichlet boundary conditions on the outside boundary. The interface boundary conditions are found as follows.

The coefficients in the Hamiltonians are step functions (a different constant in each material) so the differential equations only make sense in the weak formulation. To show how to find the interface boundary conditions compatible with the weak formulation we look at a one-band Hamiltonian for a quantum well oriented in the [100] direction at the zone center, i.e. we have to solve

$$\frac{\partial}{\partial x}A\frac{\partial}{\partial x}\phi = E\phi,$$

for ϕ and E, where A is a step function. The weak formulation of this problem is to find ϕ and E such that

$$\int_\Omega \psi\frac{\partial}{\partial x}A\frac{\partial}{\partial x}\phi \mathrm{d}^3r = E\int_\Omega \psi\phi \mathrm{d}^3r \quad \forall\,\psi\in C_0^\infty(\Omega), \tag{2}$$

where the subscript signifies that the functions have compact support. The region Ω is split into two regions Ω_1 and Ω_2, where Ω_1 is the barrier material and Ω_2 is the well material and ϕ_i is the limit of ϕ taken from region Ω_i. Using integration by parts we see that

$$\int_\Omega \psi\frac{\partial}{\partial x}A\frac{\partial}{\partial x}\phi \mathrm{d}^3r = -\int_\Omega \frac{\partial}{\partial x}(\psi)A\frac{\partial}{\partial x}\phi \mathrm{d}^3r$$

$$= -A_1\int_{\Omega_1}\frac{\partial}{\partial x}(\psi)\frac{\partial}{\partial x}\phi \mathrm{d}^3r - A_2\int_{\Omega_2}\frac{\partial}{\partial x}(\psi)\frac{\partial}{\partial x}\phi \mathrm{d}^3r$$

$$= A_1\int_\Omega \psi\frac{\partial}{\partial x}\frac{\partial}{\partial x}\phi \mathrm{d}^3r + A_2\int_\Omega \psi\frac{\partial}{\partial x}\frac{\partial}{\partial x}\phi \mathrm{d}^3r$$

$$+A_2\int_{\partial_{12}} n_x\psi\frac{\partial}{\partial x}\phi_2 \mathrm{d}A - A_1\int_{\partial_{12}} n_x\psi\frac{\partial}{\partial x}\phi_1 \mathrm{d}A,$$

where n_x is the x component of the outward unit normal and ∂_{12} is the boundary between Ω_1 and Ω_2. With the help of this, we can rewrite Eq. (2) as follows. Find ϕ and E such that

$$A_1\frac{\partial}{\partial x}\frac{\partial}{\partial x}\phi = E\phi \quad \text{in} \quad \Omega_1, \quad A_2\frac{\partial}{\partial x}\frac{\partial}{\partial x}\phi = E\phi \quad \text{in} \quad \Omega_2,$$

with Neumann boundary conditions on the interface between Ω_1 and Ω_2. A similar derivation can be carried out for the four-band Hamiltonians again arriving at Neumann interface boundary conditions.

On the basis of this we can draw the following conclusion. We know that the two Hamiltonians are identical in bulk materials, which gives us that it is only the interface boundary conditions that makes the two models different, and this difference is exactly the extra terms proportional to C_1+C_2. Notice that it is because we have differential operators in front of the step functions that we have this difference. A similarly result was arrived at recently by Boujdaria et al. [20].

2.3. Orientation

In this section we explain how to derive the Hamiltonian for a quantum wire oriented in an arbitrary direction starting from a three-dimensional Hamiltonian. The system we are investigating is an embedded quantum wire oriented along the z' direction (see Fig. 1). We start with the Hamiltonian written in terms of the $|X\rangle$, $|Y\rangle$, $|Z\rangle$ basis with respect to the Cartesian coordinate system x, y, z along the [100], [010] and [001] directions respectively:

$$H_{\alpha\beta}(\vec{k}) = \sum_{ij} k_i D^{ij}_{\alpha\beta} k_j,$$

where

$$\frac{2m}{\hbar^2}D_{11} = k_xAk_x + k_yBk_y + k_zBk_z, \tag{3}$$

$$\frac{2m}{\hbar^2}D_{22} = k_xBk_x + k_yAk_y + k_zBk_z,$$

$$\frac{2m}{\hbar^2}D_{33} = k_xBk_x + k_yBk_y + k_zAk_z,$$

$$\frac{2m}{\hbar^2}D_{12} = \frac{1}{2}[k_x(C_1-C_2)k_y + k_y(C_1-C_2)k_x]$$

$$+\frac{1}{2}[k_x(C_1+C_2)k_y - k_y(C_1+C_2)k_x],$$

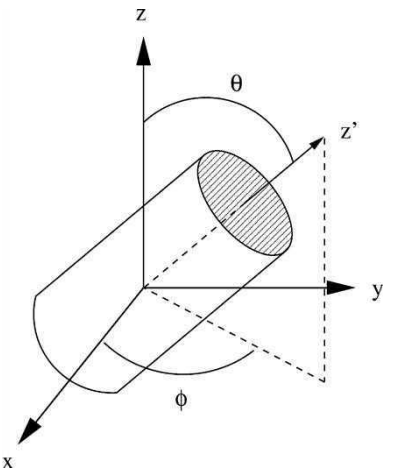

Fig. 1. A quantum wire oriented in the z' direction.

$$\frac{2m}{\hbar^2}D_{13} = \frac{1}{2}[k_x(C_1 - C_2)k_z + k_z(C_1 - C_2)k_x] + \frac{1}{2}[k_x(C_1 + C_2)k_z - k_z(C_1 + C_2)k_x],$$

$$\frac{2m}{\hbar^2}D_{23} = \frac{1}{2}[k_y(C_1 - C_2)k_z + k_z(C_1 - C_2)k_y] + \frac{1}{2}[k_y(C_1 + C_2)k_z - k_z(C_1 + C_2)k_y].$$

The rest can be found by using that the Hamiltonian is hermitian.

In order to use the translational symmetry in the z' direction, we introduce the rotation matrix U that rotates the xyz axes onto the $x'y'z'$ axes:

$$x'_j = U_{ji}x_i, \quad k'_j = U_{ji}k_i,$$

where

$$U(\phi,\theta) = \begin{pmatrix} \cos(\phi)\cos(\theta) & \sin(\phi)\cos(\theta) & -\sin(\theta) \\ -\sin(\phi) & \cos(\phi) & 0 \\ \cos(\phi)\sin(\theta) & \sin(\phi)\sin(\theta) & \cos(\theta) \end{pmatrix}$$

See Fig. 1 for a definition of the angles θ and ϕ. Using this, we can write the Hamiltonian in terms of the primed basis functions $|X''\rangle$, $|Y''\rangle$, $|Z''\rangle$ with respect to the new primed coordinate system.

$$H'_{\alpha'\beta'}(\vec{k'}) = \sum_{\alpha\beta}\sum_{ij}\sum_{i'j'} U_{\alpha'\alpha}U_{\beta'\beta}U_{i'i}U_{j'j}k_{i'}D^{ij}_{\alpha\beta}k_{j'}. \tag{4}$$

We can now use the translational symmetry to write the envelope functions as follows.

$$\mathbf{F}(x',y',z') = \mathrm{e}^{\mathrm{i}k'_z z'}\tilde{\mathbf{F}}(x',y'),$$

where k'_z is a constant. This reduces the model to a two-dimensional problem. The four-band model is found by including the spin-orbit contribution, shifting to the *JM* basis and only keeping the heavy and light hole contributions.

To see the influence of the orientation on the difference between the two Hamiltonians, we derive the difference (the terms proportional to C_1+C_2) for an arbitrary orientation. First note that $\mathcal{D}^{ij}_{\alpha\beta}$ is zero except when $i=\alpha$ and $j=\beta$ or $i=\beta$ and $j=\alpha$, where $\mathcal{D}^{ij}_{\alpha\beta}$ are the terms proportional to C_1+C_2 (see Eq. (3)). In addition we note that all the $\mathcal{D}^{\alpha\beta}_{\alpha\beta}$s are equal and the same is true for $\mathcal{D}^{\beta\alpha}_{\alpha\beta}$. Using this we get

$$\mathcal{D}'_{\alpha'\beta'}(\vec{k'}) = \sum_{\alpha\beta}\sum_{ij}\sum_{i'j'} k_{i'}U_{\alpha'\alpha}U_{\beta'\beta}U_{i'i}U_{j'j}\mathcal{D}^{ij}_{\alpha\beta}k_{j'}$$

$$= \sum_{\alpha\beta}\sum_{i'j'} k_{i'}U_{\alpha'\alpha}U_{\beta'\beta}U_{i'\alpha}U_{j'\beta}\mathcal{D}^{\alpha\beta}_{\alpha\beta}k_{j'} + k_{j'}U_{\alpha'\alpha}U_{\beta'\beta}U_{i'\beta}U_{j'\alpha}\mathcal{D}^{\beta\alpha}_{\alpha\beta}k_{j'}$$

$$= k_{\alpha'}\mathcal{D}^{\alpha'\beta'}_{\alpha'\beta'}k_{\beta'} + k_{\beta'}\mathcal{D}^{\beta'\alpha'}_{\alpha'\beta'}k_{\alpha'}$$

$$= \sum_{ij'} k_{i'}\mathcal{D}^{i'j'}_{\alpha'\beta'}k_{j'}.$$

That is, the difference between the two Hamiltonians is independent of the orientation of the wire. This surprising result can be understood by noting that [6]

$$C_1 + C_2 = 2(1 + \gamma_1 - 2\gamma_2 - 3\gamma_3) = 2(1 + \gamma_1) - 5\gamma_1\mu,$$

where the γ_i's are the Luttinger parameters and μ is known as the spherical parameter [21]. Hence, the combination C_1+C_2, being independent of the parameter δ which is responsible for the warping in the valence bands of zincblende materials [21], has spherical symmetry. So if we see a large difference in the energy bands for one orientation, we would expect to find a large difference for any other orientation.

One way of studying the influence of orientation on the band structure is to find the symmetry groups for each orientation. This tells us whether or not we can expect any degeneracy as well as indicate in which cases we can have crossings or anti-crossings between different energy dispersion curves. The degeneracy resulting from symmetry is given by the dimension of the irreducible representations of the point groups, and we expect to see anti-crossings between energy dispersion curves belonging to the same irreducible representations and crossings otherwise. The crystal point groups were found as the subgroups of the zinc blende point group T_d that left the quantum wire unchanged. The point groups for the four-band Hamiltonian were found by checking which rotations and reflections left the Hamiltonian unchanged, again only with respect to the symmetry operations that left the quantum wire unchanged as well. In Table 2, we list the point groups for the four-band Hamiltonian (they are the same for LK and BF). Table 3 shows the crystal point groups for the different orientations and structures. From these two tables, we see that the four-band point groups can be found from the crystal point groups by adding inversions to the group except for the triangular structure. The triangular structure is special because it does not allow inversion.

In Tables 4 and 5, we show the group of wave vector for the four-band Hamiltonian and the crystal, respectively. The group of wave vector is just the subgroup that leaves k_z unchanged, that is, gives the symmetry away from the zone center, From compatibility table (see Ref. [22], we see that

Table 2
Point groups for the four-band Hamiltonian

	[001]	[110]	[111]
Circle	D_{4h}	D_{2h}	D_{3d}
Square	D_{4h}	D_{2h}	C_{2h}
Triangle	C_{2v}	C_{2v}	C_3

Table 3
Crystal point groups

	[001]	[110]	[111]
Circle	D_{2d}	C_{2v}	C_{3v}
Square	D_{2d}	C_{2v}	C_{3v}
Triangle	C_2	C_s	C_3

the four-band Hamiltonian may not capture all the physics of a quantum wire oriented in the [110] direction. The reason for this is that a double degenerate state calculated with the four-band Hamiltonian may split if we take into account crystal symmetry ($\Gamma_5 \rightarrow \Gamma_3 + \Gamma_4$ with respect to the C_s group), i.e. group theory tells us that the four-band Hamiltonian has a double degenerate state that split under the reduced crystal symmetry group.

3. Results

In this section we present results for the following system characteristics:

- shape (circular, square and triangular),
- orientation ([001], [110], [111]),
- size of the quantum wire (circle with a diameter of 6 and 10 nm) and
- material system (GsAs/AlAs, $In_{0.53}Ga_{0.47}As/InP$).

We have made calculations for all possible combinations of these characteristics, but we will only present the most significant results here.

3.1. Shape and orientation

We have studied the three different quantum wire cross-sectional shapes shown in Fig. 2.

The length scales are chosen such that all the shapes have the same cross-sectional area and the triangle is equilateral.

In Fig. 3, we show results for GaAs/AlAs quantum wires oriented in the [001] direction. We see that the shape has no significant influence on the difference between the band structures calculated with the two Hamiltonians and within the part of the Brillouin zone shown the difference is at most 10 meV. Notice also that there is a difference between the two models at the Brillouin zone center.

When we compare the dispersion curves for the circle and the square, we see that they are more or less the same.

Table 4
Groups of the wave vector for the four-band Hamiltonian

	[001]	[110]	[111]
Circle	C_{4v}	C_{2v}	C_{3v}
Square	C_{4v}	C_{2v}	C_s
Triangle	C_s	C_s	C_3

Table 5
Crystal groups of the wave vector

	[001]	[110]	[111]
Circle	C_{2v}	C_s	C_{3v}
Square	C_{2v}	C_s	C_s
Triangle	C_1	C_1	C_3

This is in accordance with the group Tables 2 and 4 which show that they have the same symmetry. When we look at the dispersion curves for the triangle, we see a marked difference from the circle and the square, we even have a splitting of the degeneracy away from $k_z=0$. This is because we do not have inversion symmetry in this case and it is also apparent from the symmetry group tables.

We have also carried out calculations for the following three orientations, [001], [110] and [111], and the results of these calculations are shown in Fig. 4. The wire chosen was a GaAs/AlAs circular quantum wire with a 6 nm diameter.

We see, as was expected, that the orientation has no discernible influence on the difference between the results obtained with the two Hamiltonians. Again we see a difference of at most 10 meV between BF and LK.

We also observe that in the [001] and [111] direction the dispersion curves cross whereas in the [110] direction they do not cross. This can be explained with the help of the group table. Here we see that the symmetry group for the [110] directions only have one irreducible representation compatible with spin 1/2, so we would expect to see crossings. The groups for the [001] and [111] directions have, on the other hand, more than one irreducible representation and we would, because of that, expect to see anti-crossings.

3.2. Size and material system

In Fig. 5, we show results for GaAs/AlAs circular quantum wires with diameters of 6 and 10 nm, respectively.

We notice that the difference between the two models does depend on the size of the quantum wire. This is in agreement with the results by Pokatilov et al. [5]. In the case of the wire with a 6 nm diameter, the difference is up to 10 meV, whereas in the 10 nm case the difference is only up to 4 meV. The reason for this is that as the size of the wire is decreased the envelope function will feel the interface more and more (see Fig. 5(b)). And, as we mentioned in Section 2, it is only the interface boundary conditions that differ from model to model. We also see that the spacing between dispersion curves is larger for the smaller structure compared to the larger structure. This is a well-known confinement effect.

In Fig. 6, we show energy dispersion curves for two different material systems, GaAs/AlAs and $In_{0.53}Ga_{0.47}As/InP$. The material parameters are given in Table 1 and the coefficients that are used in the Hamiltonians are given in terms of the Luttinger parameters as follows [6]:

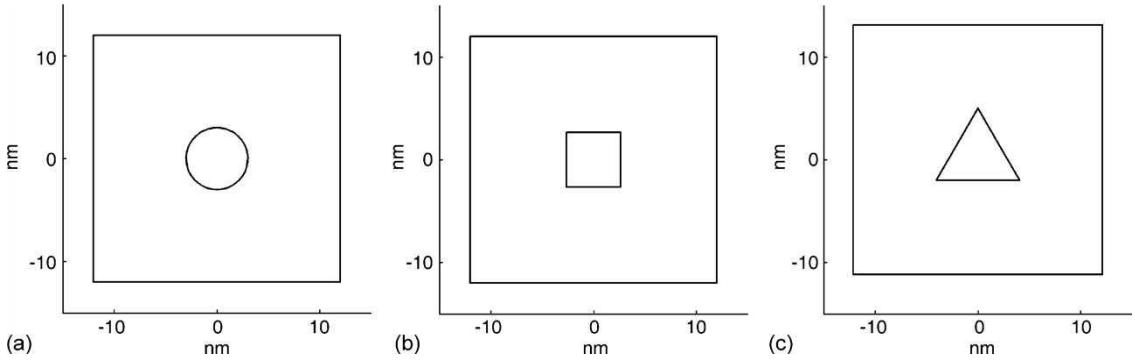

Fig. 2. Quantum-wire cross-sectional shapes. (a) Circle with a 6 nm diameter, (b) square with a 5.3 nm side and (c) triangle with a 8 nm baseline.

$$A = 1 - 6\sigma - 12\delta = -(\gamma_1 + 4\gamma_2), \quad B = 1 - 6\pi$$
$$= -(\gamma_1 - 2\gamma_2), \quad C_1 = 6\delta - 6\sigma$$
$$= 1 + \gamma_1 - 2\gamma_2 - 6\gamma_3, \quad C_2 = 6\pi$$
$$= 1 + \gamma_1 - 2\gamma_2. \tag{5}$$

From the dispersion curves shown, we see that the difference between the LK and the BF Hamiltonians depends strongly on the material system. For the $In_{0.53}Ga_{0.47}As/InP$ quantum wire, there is a difference of up to 30 meV compared with a difference of only up to 4 meV for the GaAs/AlAs quantum wire. The reason for this is, as we mentioned in Section 2, that the difference between the two models is characterized by the step function C_1+C_2 alone and it also only depends on the interface boundary conditions. From these two facts we can infer that the difference is characterized by the difference in C_1+C_2 between the two materials. And from Table 1, we see that this difference is 19.84 for the $In_{0.53}Ga_{0.47}As/InP$ system, whereas it is only 8.54 for the GaAs/AlAs system.

4. Conclusion

We have presented a general way to derive a multiband Hamiltonian, that uses the translational symmetry, for a quantum wire with an arbitrary orientation starting from a three-dimensional multiband Hamiltonian. This was used to show that the difference between the LK and the BF Hamiltonians is invariant with respect to orientation. We have also shown calculated dispersion curves for quantum wires with different shapes, orientations, sizes and different materials composition. These reveal that the difference

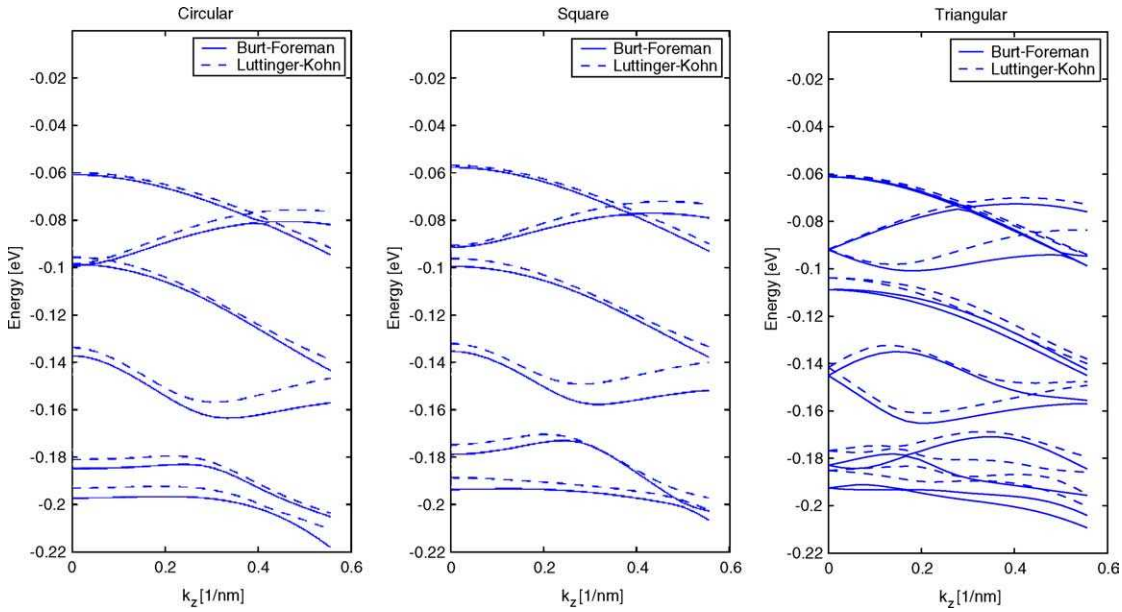

Fig. 3. Dispersion curves for GaAs/AlAs quantum wires with circular, square and triangular cross-section, respectively, all oriented in the [001] direction.

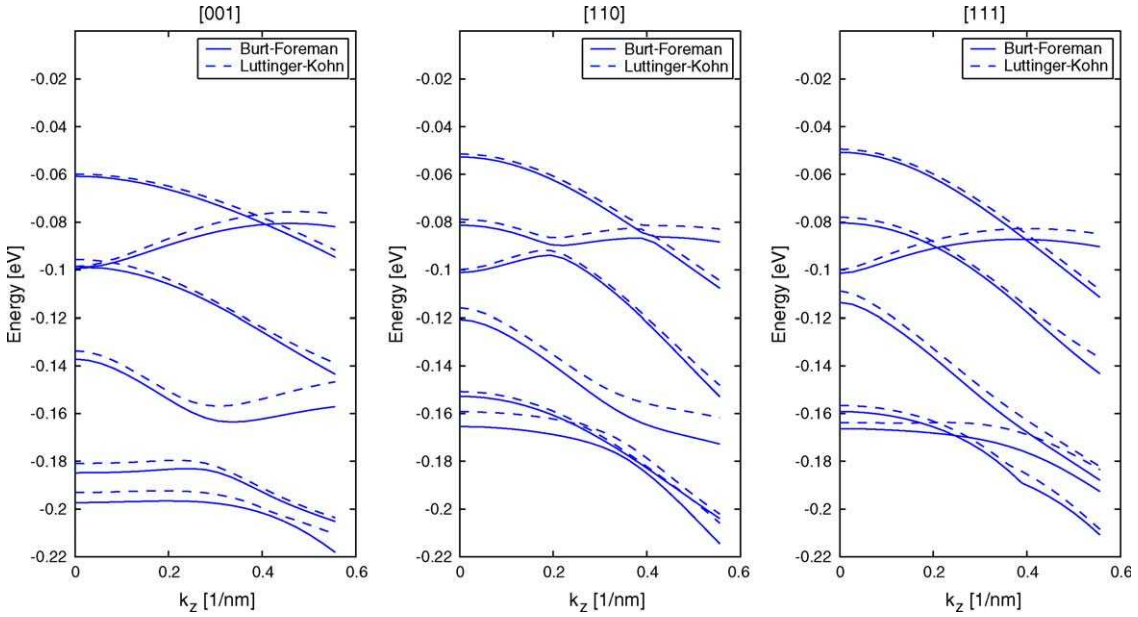

Fig. 4. Energy dispersion curves for a GaAs/AlAs circular quantum wire with a 6 nm diameter in the [001], [110] and [111] directions.

between LK and BF is more or less independent of shape and orientation but it does depend on the size of the structure and the material composition. We saw that the smaller the structure and the larger the difference in $C_1 + C_2$ between the two materials the more of a difference was observed. In addition to this, we also presented the symmetry groups for the different systems under investigation both for the four-band Hamiltonian and for the crystal. This was used to describe some of the results obtained with the four-band Hamiltonians.

Acknowledgements

LCLYV acknowledges support from NSF-DMR (Grant No. 9984059), Mads Clausen Foundation, and Balslev Fond.

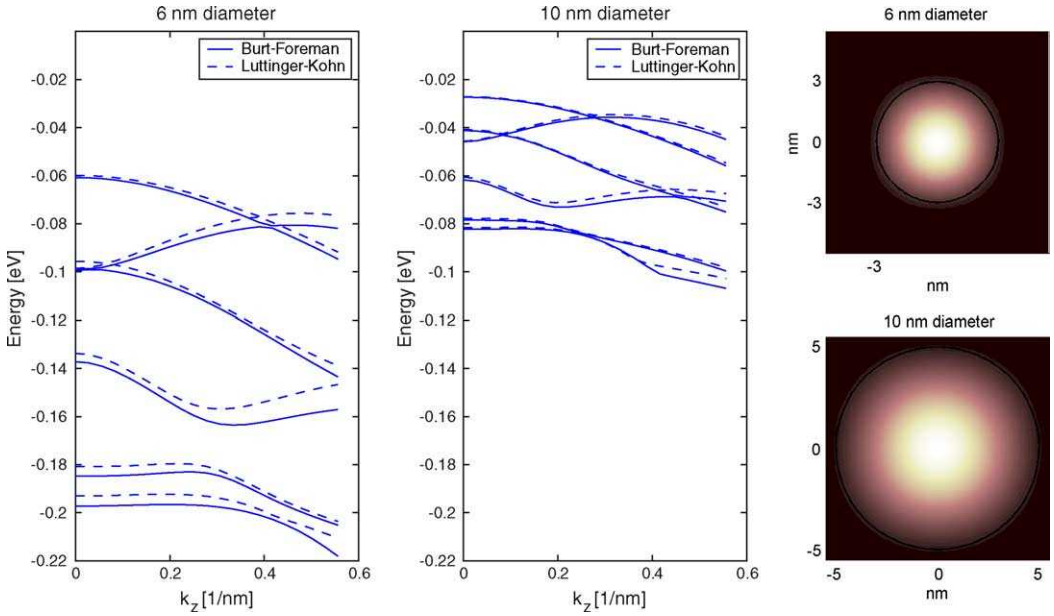

Fig. 5. (a) Energy dispersion curves for two GaAs/AlAs circular quantum wires oriented in the [001] direction with a diameter of 6 and 10 nm respectively and, (b) ground-state probability densities for the two wires ($\sum_n \tilde{F}_n^2$).

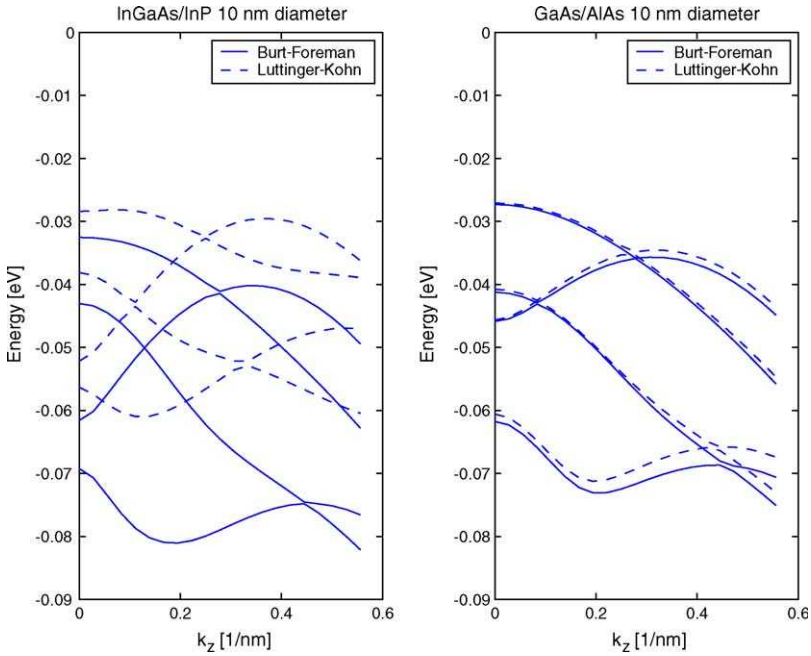

Fig. 6. Dispersion curves for circular quantam wires with a 10 nm diameter oriented in the [001] direction.

The authors would also like to thank Prof. Cardona for pointing out the connection between the $C_1 + C_2$ parameter and the spherical parameters.

References

[1] M.G. Burt, The justification for applying effective-mass approximation to microstructures, J. Phys. Condens. Matter 4 (1992) 6651–6690.
[2] J.M. Luttinger, W. Kohn, Motion of electron and holes in perturbed periodic fields., Phys. Rev. 97 (1955) 869.
[3] A.T. Meney, Besire Gonul, E.P. O'Reilly, Evaluation of various approximations used in the envelope-function method., Phys. Rev. B 50 (1994) 10893.
[4] F. Mireles, E. Ulloa, Ordered Hamiltonian and matching conditions for heterojunctions with wurtzite symmetry: GaN/Al_x Ga_{1-x}N quantum wells, Phys. Rev. B 60 (1999) 13659.
[5] E.P. Pokatilov, V.A. Fonoberov, V.M. Fomin, T. Devreese, Development of an eight-band theory for quantum dot heterostructures, Physical Review B 64 (2001) 245328.
[6] R. van Dalen, P.N. Stavrinou, General rules for constructing valence band effective mass Hamiltonian with correct operator order for heterostructures with arbitrary orientation, Semicond. Sci. Technol. 13 (1998) 11.
[7] M.A. Dupertuis, E. Martinet, D.Y. Oberli, E. Kapon, The impact of low symmetry on the electronic and optical properties of quantum wires., Europhys. Lett. 52 (2000) 420.
[8] X. Duan, C.M. Lieber, General synthesis of compound semiconductor nanowires, Adv. Mater. 12 (2000) 298.
[9] P. Ils, Ch. Greus, A. Forchel, V.D. Kulakovskii, N.A. Grippius, S.G. Tikhodeev, Linear polarization of photoluminescence emission and absorption in quantum-well wire structures: Experiment and theory, Phys Rev. B 51 (1995) 4272.
[10] M. Tsuchiya, J.M. Gaines, R.H. Yan, R.J. Simes, P.O. Holtz, L.A. Coldren, M. Petroff, Optical anisotropy in a quantum well-wire array with two-dimensional quantum confinement, Phys. Rev. Lett. 62 (1989) 466.
[11] W.E. Buhro, L. Colvin, Shape matters, Nat Mater 2 (2003) 138.
[12] D.S. Citrin, Y.-C. Chang, Valence-subband structures of GaAs/Al_xGa_{1-x}As quantum wires: the effect of split-off bands., Phys. Rev. B 40 (1989) 5507.
[13] P.C. Sercel, J. Vahala, Analytical formalism for determining quantum-wire and quantum-dot band structure in the multiband envelope-function approximation, Phys. Rev. B 42 (1990) 3690.
[14] I. Vurgaftman, J.M. Hinckley, J. Singh, A comparison of optoelectronic properties of lattice-matched and strained quantum-well and quantum-wire structures, IEEE J. Quantum Electron 30 (1994) 75.
[15] C. Galeriu, L.C. Lew Yan Voon, M. Willatzen, Modelling intersubband transitions in the valence bands of quantum-well structures in: H. Sigg (Ed.), Proceeding of the Workshop on Intersubband Transitions in Quantum wells (2003).
[16] B. Lassen, L.C. Lew Yan Voon, R. Melnik, M. Willatzen, Valence-band energies of GaAs/AlAs and InGaAs/InP V-groove [1$\bar{1}$0] quantum wires, Proc. Nanotech-2004 3:34, (2004).
[17] B. Lassen, R. Melnik, M. Willatzen, L.C. Lew Yan Voon, Differences between Luttinger–Kohn and exact envelope function approaches for quantum-wire electronic bandstructures in: H. Sigg (Ed.), Proceeding of the Workshop on Intersubband Transitions in Quantum wells (2003).

[18] Numerical Data and Functional Relationships in Science and Thechnology, in: K.H. Hellwege (Ed.), Landolt-Börnstein vol. 22a, Springer, Berlin, 1982 New Series, Group III.
[19] S.A. Stoklitsky, Q.X. Zhao, P.O. Holtz, B. Monemar, T. Lundström, Optical intervalence-subband transitions in strained p-type $In_{1-x}Ga_xAs/InP$ quantum wells, J. Appl. Phys 77 (1995) 5256.
[20] K. Boujdaria, S. Ridene, S. Ben Radhia, H. Bouchriha, G. Fishman, Symmetrized Hamiltonian versus 'foreman' Hamiltonian for semiconductor valence band: an insight, Solid State Commun 129 (3) (2004) 221–226.
[21] P.Y. Yu, M. Cardona, Fundamentals of Semiconductors, 1st ed., Springer, 1996.
[22] G.F. Koster, J.O. Dimmock, R.G. Wheeler, H. Statz, Properties of the Thirty-Two Point Groups, M.I.T. Press, Cambridge, MA, USA, 1963.